creative commons
COMMONS DEED

저작자표시-비영리-변경금지 2.0 대한민국

이용자는 아래의 조건을 따르는 경우에 한하여 자유롭게

- 이 저작물을 복제, 배포, 전송, 전시, 공연 및 방송할 수 있습니다.

다음과 같은 조건을 따라야 합니다:

저작자표시. 귀하는 원저작자를 표시하여야 합니다.

비영리. 귀하는 이 저작물을 영리 목적으로 이용할 수 없습니다.

변경금지. 귀하는 이 저작물을 개작, 변형 또는 가공할 수 없습니다.

- 귀하는, 이 저작물의 재이용이나 배포의 경우, 이 저작물에 적용된 이용허락조건을 명확하게 나타내어야 합니다.
- 저작권자로부터 별도의 허가를 받으면 이러한 조건들은 적용되지 않습니다.

저작권법에 따른 이용자의 권리는 위의 내용에 의하여 영향을 받지 않습니다.

이것은 이용허락규약(Legal Code)을 이해하기 쉽게 요약한 것입니다.

Disclaimer

dCollection

임상의과학과 석사 학위논문

Prediction of microvascular invasion of hepatocellular carcinoma: value of volumetric iodine quantification using preoperative dual-energy computed tomography

간세포암의 미세혈관침습 예측: 수술 전 이중에너지 전산화 단층촬영을 이용한 용적화된 요오드 정량화의 가치

2020 년 8 월

서울대학교 의과대학원
임상의과학과
김 택 민

임상의과학과 석사 학위논문

Prediction of microvascular invasion of hepatocellular carcinoma: value of volumetric iodine quantification using preoperative dual-energy computed tomography

간세포암의 미세혈관침습 예측: 수술 전 이중에너지 전산화 단층촬영을 이용한 용적화된 요오드 정량화의 가치

2020 년 8 월

서울대학교 의과대학원
임상의과학과
김 택 민

간세포암의 미세혈관침습 예측:
수술 전 이중에너지 전산화 단층촬영을 이용한 용적화된 요오드 정량화의 가치

지도교수 이 정 민

이 논문을 임상의과학과 석사 학위논문으로 제출함

2020 년 5 월

서울대학교 의과대학원

임상의과학과

김 택 민

김택민의 석사 학위논문을 인준함

2020 년 7 월

위 원 장 조 정 연 (인)

부 위 원 장 이 정 민 (인)

위 원 이 남 준 (인)

ABSTRACT

Prediction of microvascular invasion of hepatocellular carcinoma: value of volumetric iodine quantification using preoperative dual-energy computed tomography

Taek Min Kim

Department of Clinical Medical Sciences

Graduate School of Medicine

Seoul National University

Objective

To investigate the potential value of volumetric iodine quantification using preoperative dual-energy computed tomography (DECT) for predicting microvascular invasion (MVI) of hepatocellular carcinoma (HCC).

Materials and Methods

This retrospective study included patients with single HCC treated through surgical resection who underwent preoperative DECT. Quantitative DECT features, including normalized iodine concentration (NIC) to the aorta and mixed-energy CT attenuation value in the arterial phase, were three-dimensionally measured for peritumoral and intratumoral regions: (i) layer-by-layer analysis for peritumoral layers (outer layers 1 and 2; numbered in close order from the tumor boundary) and intratumoral layers (inner layers 1 and 2) with 2-mm layer thickness and (ii) volume of interest (VOI)-based analysis with different volume coverage (tumor itself; VOI_{O1}, tumor plus outer layer 1; VOI_{O2}, tumor plus outer layers 1 and 2; VOI_{I1}, tumor minus inner layer 1; VOI_{I2}, tumor minus inner layers 1 and 2). In addition, qualitative CT features, including peritumoral enhancement and tumor margin, were assessed. Qualitative and quantitative CT features were compared between HCC patients with and without MVI. Diagnostic performance of DECT parameters of layers and VOIs was assessed using receiver operating characteristic curve analysis.

Results

A total of 36 patients (24 men, mean age 59.9 ± 8.5 years) with MVI (n = 14) and without MVI (n = 22) were included. HCCs with MVI showed significantly higher NICs of outer layer 1, outer layer 2, VOI_{O1}, and VOI_{O2} than those without MVI (P = 0.01, 0.04, 0.02, 0.02, respectively). Among the NICs of layers and VOIs, the highest area under the curve was obtained in outer layer 1 (0.747). Qualitative features, including peritumoral enhancement and tumor margin, and the mean CT attenuation of each layer and each VOI were not significantly different between HCCs with and without MVI (both $P > 0.05$).

Conclusion

Volumetric iodine quantification of peritumoral and intratumoral regions using DECT may help predict the MVI of HCC.

Keywords

Hepatocellular carcinoma, Microvascular invasion, Dual-energy CT, Peritumoral enhancement, Iodine quantification, Iodine concentration

Student Number: 2017-20656

Contents

List of Tables and Figures

Table 8. Intraobserver and interobserver agreements of quantitative and qualitative parameters.

Figure 1. Flow diagram of patient selection for the study.

Figure 2. Semiautomatic volumetric segmentation of the hepatocellular carcinoma (HCC)

(a) HCC demonstrated in the mixed-energy images. (b) Readers manually draw a line across the maximum dimension of the tumor. (c) The software automatically segments the entire tumor volume. (d) Coronal reconstructed image shows the volumetric tumor segmented in three dimensions

Figure 3. Representative images of the layers and volume of interest (VOIs)

(a) Original mixed-energy images. (b) Layer-by-layer analysis for two peritumoral layers (outer layer 1 [yellow], outer layer 2 [green]) and two intratumoral layers (inner layer 1 [orange], inner layer 2 [blue]) with a 2-mm layer thickness. (c) VOI of the tumor. (d) VOI_{O1}, tumor plus outer layer 1. (e) VOI_{O2}, tumor plus outer layers 1 and 2. (f) VOI_{I1}, tumor minus inner layer 1. (g) VOI_{I2}, tumor minus inner layers 1 and 2. (h) The aforementioned analysis performed in the same manner with a 4-mm layer thickness.

Figure 4. Receiver operating characteristic curves to evaluate the diagnostic performance of normalized iodine concentrations of peritumoral regions to identify microvascular invasion in (a) layers and (b) volume of interests.

Figure 5. A 64-year-old man with hepatocellular carcinoma (HCC) without microvascular invasion (MVI).

(a) Enhancing area found in the peritumoral area (arrows) adjacent to the HCC (arrowheads) in the arterial phase, which became (b) isoattenuation in the equilibrium phase. However, the NIC of the peritumoral layer with a 2-mm distance from the tumor margin is 0.03 mg/mL, lower than 0.082 mg/mL, which is the cutoff value for identifying MVI

Figure 6. A 54-year-old man with hepatocellular carcinoma (HCC) with microvascular invasion (MVI).

(a) No definite peritumoral enhancement found around HCC (arrowheads) in the arterial phase compared with (b) equilibrium phase images. However, the NIC of the peritumoral layer with a 2-mm distance from the tumor margin is 0.096 mg/mL, which is higher than the cutoff value for predicting MVI of 0.082 mg/mL

Introduction

Hepatocellular carcinoma (HCC) is the most common primary liver cancer and is the second leading cause of cancer-related deaths in the Asia-Pacific region (1). Liver resection and liver transplantation are the first-line curative treatments for eligible patients, but recurrence after surgical treatment is frequent. Previous studies have reported a 5-year recurrence rate of 25% after liver transplantation and 70% after liver resection (2, 3). Vascular invasion is a prognostic factor for predicting recurrence and overall survival (4). In particular, microvascular invasion (MVI) is known to be responsible for early recurrence within the first two years after curative treatments (5). Thus, we may be able to identify patients at risk of developing early recurrence if we can preoperatively diagnose MVI.

Previous studies reported that several imaging features of the tumor border on preoperative imaging were associated with MVI of HCC. These features include non-smooth tumor margins, peritumoral enhancement in the arterial phase, peritumoral hypointensity in the hepatobiliary phase, and radiogenomic algorithm based on the association between imaging features (internal arteries and hypoattenuating halos) (6-10). This is reasonable because, in general, a peripheral portion of many malignant tumors may have the most proliferative or aggressive biological behavior for invading adjacent parenchyma. However, preoperative MVI diagnosis is challenging, and the imaging findings and definition of “peri-” tumoral tissue are subjective and highly reader-dependent. Therefore, if we can reduce the variation and quantify the enhancement of peritumoral tissue, it would be helpful for improving the diagnostic performance of the arterial phase to identify MVI in HCC. Given that material decomposition and iodine quantification by dual-energy CT have been used for many oncologic applications, such as differentiating tumor types and assessing the treatment response of the tumor (11-14), we surmised that iodine concentration could be used for the quantitative assessment of peritumoral enhancement of HCC.

Therefore, the purpose of this study was to identify the potential diagnostic value of iodine quantification in the peritumoral region of HCC by volumetric tumor segmentation with dual-energy computed tomography (DECT) for identifying MVI.

Materials and Methods

Study population

The institutional review board of our institution approved this retrospective study and waived the requirement for informed consent. We retrospectively searched the surgical database from April 2017 and December 2019 to identify all patients who underwent hepatic resection for HCC. The patients that satisfied the following criteria were included: (a) underwent four-phase liver CT at dual-source dual-energy CT (SOMATOM Force; Siemens Healthineers, Forchheim, Germany); (b) underwent hepatic resection within 4 weeks after CT; and (c) surgically confirmed single, treatment-naïve HCC. The exclusion criteria were as follows: (a) preoperative local treatment for the index tumor; (b) < 1 cm, which may increase registration error; and (c) definite macrovascular invasion.

In the study period, 543 patients with HCC underwent hepatic resection. Of these, 472 patients did not perform preoperative liver CT at dual-source dual-energy CT within 4 weeks before surgery. Also, 28 patients who received preoperative local treatment including transarterial chemoembolization (n = 26) and transarterial radioembolization (n = 2), 4 patients who had HCC less than 1cm, and 3 patients who had HCC with macrovascular invasion were excluded. Finally, 36 patients (men/women = 24:12, mean age 59.9 ± 8.5 years) were enrolled in our study (Figure 1).

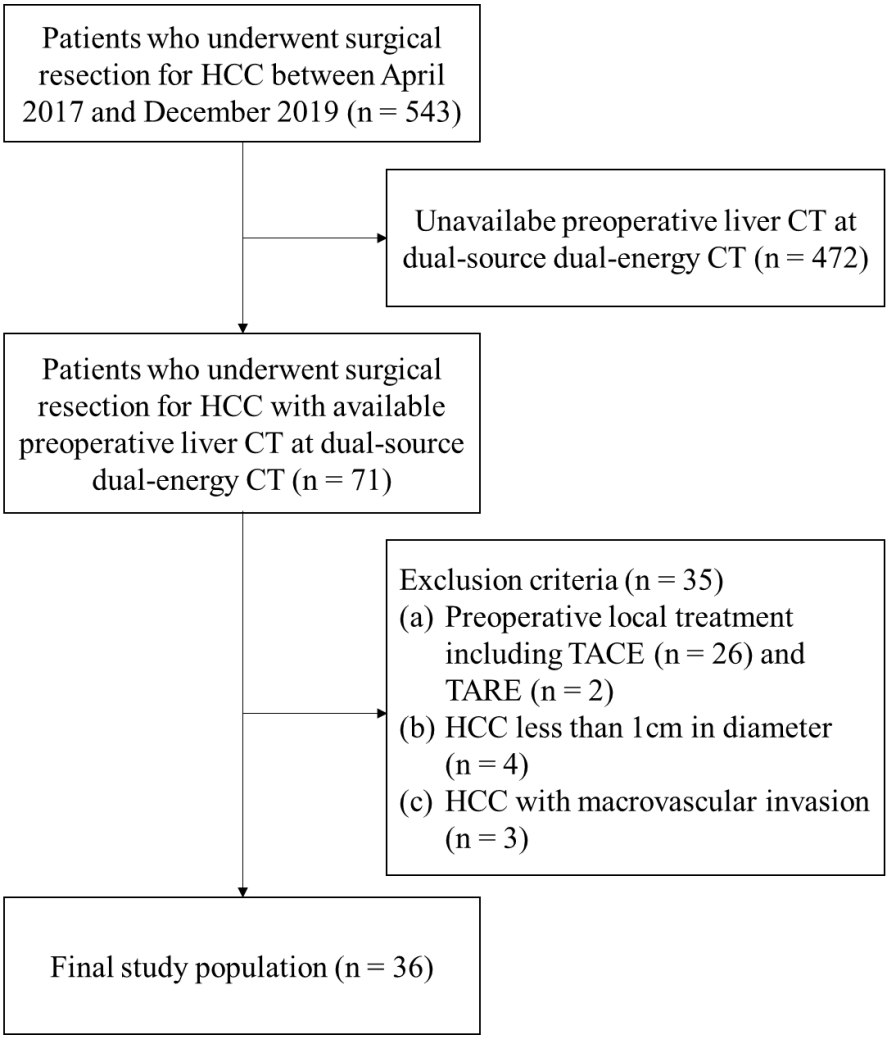

Figure 1. Flow diagram of patient selection for the study.

Abbreviations: HCC, hepatocellular carcinoma; TACE, transarterial chemoembolization; TARE, transarterial radioembolization

Histopathology

All surgical specimens were examined by experienced pathologists. The histologic parameters included size, number, Edmondson-Steiner grade, and MVI status of the resected tumor. MVI was defined as the presence of tumor cells in the portal vein, hepatic vein, or a large capsular vessel of the surrounding hepatic tissue lined by the endothelium that was visible only on microscopy.

Additionally, the histological grade of fibrosis in the background liver parenchyma was reported on the basis of the staging system for chronic hepatitis by the Korean Study Group for the Pathology of Digestive Diseases (0, no fibrosis; 1, portal fibrosis; 2, periportal fibrosis; 3, septal fibrosis; 4, cirrhosis) (15).

CT protocol

Liver CT consisted of precontrast, arterial, portal venous, and equilibrium phases. Precontrast, portal venous, and equilibrium phase images were obtained using 90-kVp tube energy before, 70 s, and 180 s after contrast media administration (iobitridol 350 mgI/mL, Xenetix® , Guerbet, France) with weight-based dosing (1.6mL/kg).

The arterial phase was scanned using dual-energy 17 s after the attenuation of the abdominal aorta reached 80 Hounsfield unit (HU) at 100 kVp, using the care bolus technique of the vendor. For arterial phase dual-energy scanning, a tube potential pair of 80/150 kV with a tin filter was used. The quality reference effective mAs was set to 250 mAs for the 80-kV tube and 125 mAs for the 150-kV tube. Detector configuration, gantry rotation time, and pitch were 192 × 0.6 mm, 0.5 s, and 0.6, respectively. Images were reconstructed with semi-smooth quantitative body kernels in all phases.

Quantitative imaging analysis

The image analysis was performed in arterial phase which was scanned in dual-energy mode. The 80- and 150-kV images of the arterial phase were imported into the prototype software (eXamine: DE Tumor Segmentation, Siemens Healthineers, Forchheim, Germany). The software loads both low- and high-kV images and automatically creates three image sets: the arterial phase of the blended images with a mixed ratio of 0.6 (60% 80 kV and 40% tin-filtered 150 kV), virtual noncontrast, and

material density iodine images. Readers identified the HCC in the mixed-volume images and drew a line across the maximum dimension of the tumor in any plane (axial, coronal, or sagittal plane). Then the software automatically segmented the entire tumor volume and calculated the tumor volume and maximal diameter (Figure 2). In addition, the following were displayed: the mean HU of mixed-energy images, total iodine concentration, and vital iodine concentration. The total iodine concentration refers to the iodine per unit volume (in milligrams per milliliter) in the entire region of interest (ROI), while vital iodine concentration refers to the iodine per unit volume in the only enhancing portion within the ROI. The tumor margin is manually edited if the tumor is not correctly segmented at once, by evaluating portal venous or equilibrium phase images.

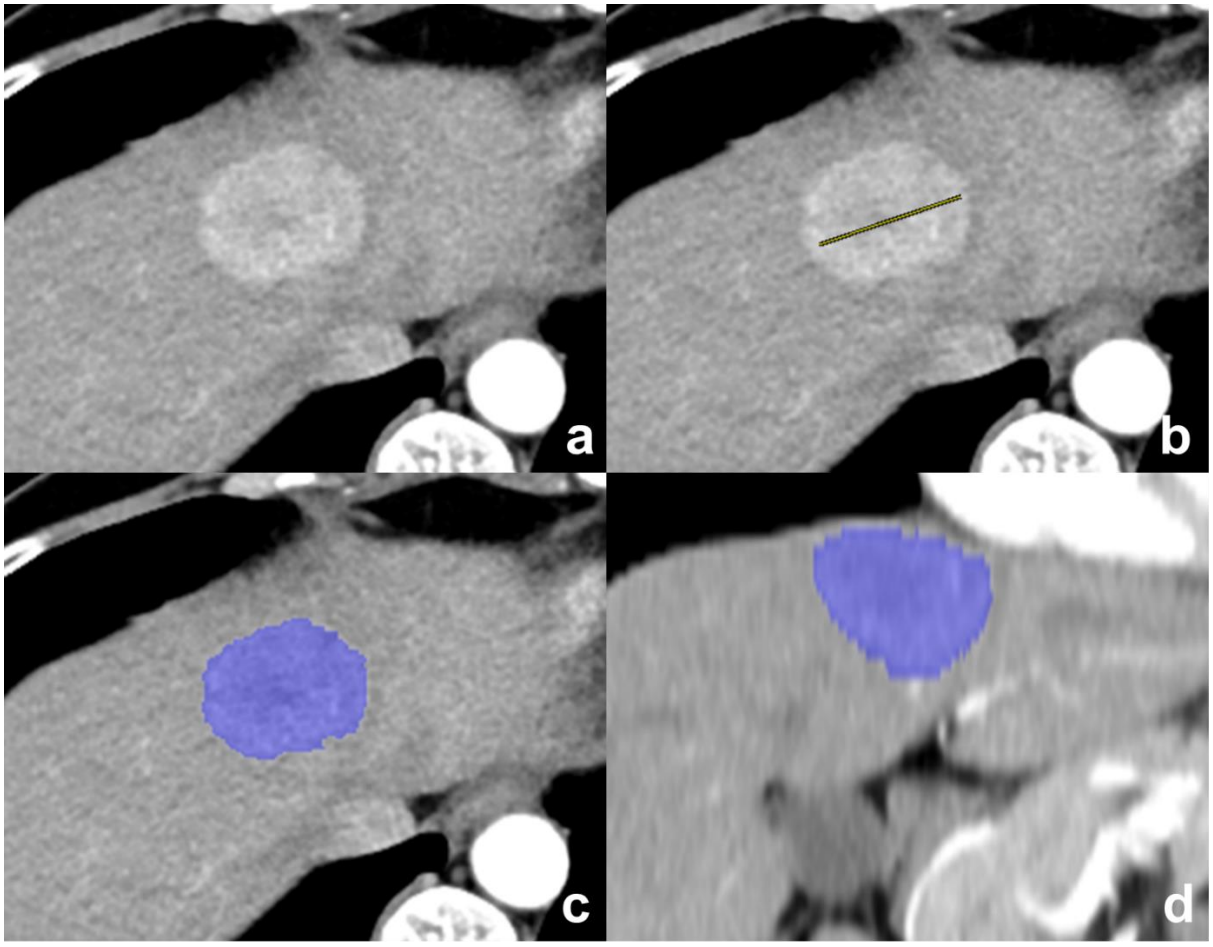

Figure 2. Semiautomatic volumetric segmentation of the hepatocellular carcinoma (HCC). (a) HCC demonstrated in the mixed-energy images. (b) Readers manually draw a line across the maximum dimension of the tumor. (c) The software automatically segments the entire tumor volume. (d) Coronal reconstructed image shows the volumetric tumor segmented in three dimensions

Subsequently, two intratumoral and two peritumoral layers from the tumor border were automatically generated using the peeling function with a layer thickness of 2 mm (outer layer 1, peritumoral region up to 2 mm from tumor margin; outer layer 2, peritumoral region from 2 mm to 4 mm from the tumor margin; inner layer 1, intratumoral region up to 2 mm from the tumor margin; inner layer 2, intratumoral region from 2 mm to 4 mm from the tumor margin). In addition, five VOIs were generated with different volume coverage (tumor itself; VOI_{O1}, tumor plus outer layer 1; VOI_{O2}, tumor plus outer layers 1 and 2; VOI_{I1}, tumor minus inner layer 1; VOI_{I2}, tumor minus inner layers 1 and 2) (Figure 3). For the layers and VOIs outside the tumor, large vessels and areas outside the liver are manually removed.

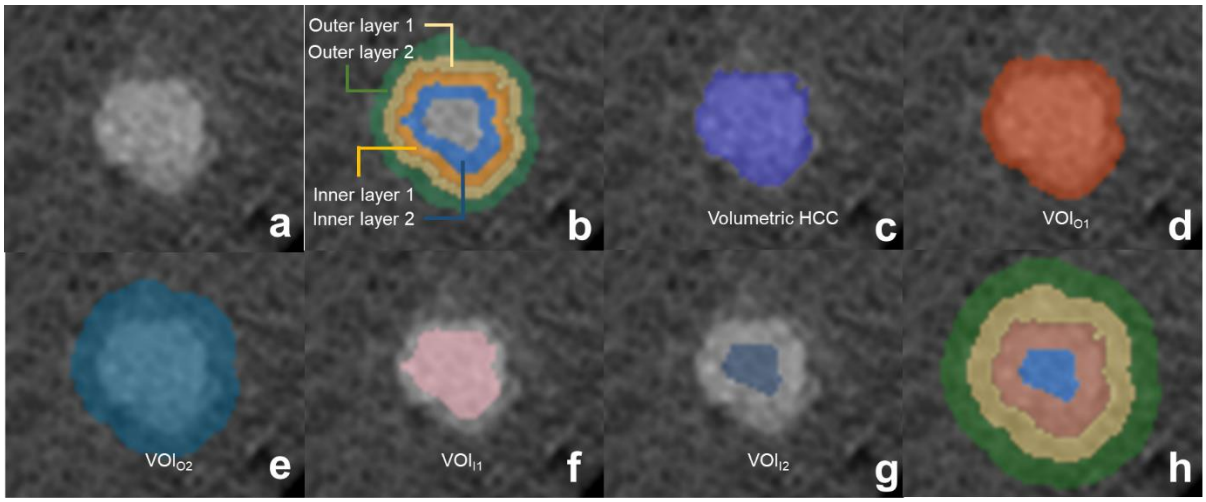

Figure 3. Representative images of the layers and volume of interest (VOIs). (a) Original mixed-energy images. (b) Layer-by-layer analysis for two peritumoral layers (outer layer 1 [yellow], outer layer 2 [green]) and two intratumoral layers (inner layer 1 [orange], inner layer 2 [blue]) with a 2-mm

layer thickness. (c) VOI of the tumor. (d) VOI_{O1}, tumor plus outer layer 1. (e) VOI_{O2}, tumor plus outer layers 1 and 2. (f) VOI_{I1}, tumor minus inner layer 1. (g) VOI_{I2}, tumor minus inner layers 1 and 2. (h) The aforementioned analysis performed in the same manner with a 4-mm layer thickness.

An ROI was manually drawn in the aorta to calculate the normalized iodine concentration (NIC) to minimize intersubject variations. The software estimates the NIC by dividing the vital iodine concentration of the ROI into the iodine concentration of the aorta. Additionally, the software automatically performs segmentation of the entire liver parenchyma to evaluate lesion-to-normal parenchyma ratios of mean attenuation by dividing the mean attenuation of the ROI into those of the normal liver parenchyma.

Measurements were performed in two separate sessions by one radiologist (---) at least 2 weeks apart and in one session by another radiologist (---) to evaluate intraobserver and interobserver reliability, respectively. The results of the first session of the former radiologist represent each participant for the other analysis in this study. In addition, the aforementioned quantitative analysis was performed in the same manner but with different layer thicknesses (4 mm) to evaluate the effect of different peritumoral or intratumoral areas.

Qualitative imaging analysis

Two fellowship-trained body radiologists (--- and ---, 6 years of liver imaging experience), who were blinded to the clinical and pathological data, independently assessed the images to evaluate the following qualitative features for MVI: (a) presence of peritumoral enhancement, which was defined as the existence of a detectable enhancing portion adjacent to the tumor border in the arterial phase, later becoming isoattenuation in the equilibrium phase (16, 17), and (b) tumor margins, whether they were smooth margins (defined as nodular tumors in all planes) or non-smooth margins

(defined as nonnodular tumors in all planes) (16, 17). All HCCs were evaluated in each dynamic phase using different planes (axial, coronal, and sagittal planes). Disagreements were resolved by consensus. One reader (---) repeated the abovementioned assessment in the same manner after 2 weeks to minimize the memory effect to evaluate intraobserver agreement.

Outcomes

Our primary end point was to evaluate the association between the NIC of peritumoral regions on DECT and MVI in HCC. Secondary end points were as follows: (a) to compare the diagnostic performance of peritumoral NIC with qualitative analysis by a human observer for identifying MVI, (b) to compare the diagnostic performance of peritumoral NIC with peritumoral mean attenuation for identifying MVI, and (c) to investigate the effect of different peritumoral areas (2 mm vs. 4 mm) on the diagnostic performance of MVI.

Statistical analysis

To compare parameters between the HCCs with and without MVI, continuous data were assessed using the Mann-Whitney test, while categorical variables were analyzed using the chi-square test. Additionally, to investigate the association between subjective peritumoral enhancement and DECT parameters of peritumoral layers, the mean attenuation and layer-to-normal parenchyma ratio of mean attenuation of peritumoral layers were compared between the groups with absent and present peritumoral enhancement. A receiver operating characteristic (ROC) curve analysis was performed using quantitative parameters of layers and VOIs and qualitative parameters to determine the diagnostic performance for the prediction of MVI. Areas under the ROC curves (AUCs) with 95% confidence intervals (CIs) were calculated for the significant CT parameters, and a comparison

analysis of AUCs was performed. Variables with $P < 0.10$ in univariate analysis were applied to binary logistic regression analysis. Continuous variables were converted to categorical variables with optimal cutoff values to perform multivariate analysis. Among the NIC of multiple layers and VOIs, only one layer or VOI that showed the highest AUC was included in the multivariate analysis to avoid multicollinearity of parameters.

Intraobserver and interobserver agreements were evaluated using intraclass coefficient class (ICC) and Cohen κ-statistics. The strength of agreement via ICC and κ values <0.4, 0.4–0.6, 0.6–0.8, and >0.8 were categorized poor, moderate, good, and excellent agreement, respectively. Statistical analyses were performed using a statistical software package (SPSS version 23, SPSS, Inc., Chicago, IL). Differences of $P < 0.05$ were considered statistically significant.

Results

Patient characteristics

A total of 36 HCCs with MVI (n = 14) and without MVI (n = 22) were included. The median tumor size was 2.5 cm (range, 1.2–4.5 cm). The surgical procedures included segmentectomy (n = 23), right anterior sectionectomy (n = 1), left lateral sectionectomy (n = 3), right hemihepatectomy (n = 2), left hemihepatectomy (n = 3), and total hepatectomy for transplantation (n = 4). The mean time between dual-energy CT and surgery was 16 days (range, 1–30 days). The detailed information of the study group is summarized in Table 1.

Between the two groups with and without MVI, no significant difference was observed in age, sex, histologic grade of hepatic fibrosis, underlying liver disease, and Edmondson-Steiner grade of HCCs ($P > 0.05$, Table 1). Tumor size did not differ between the two groups with and without MVI (3 ± 1.3 cm vs. 2.5 ± 0.9 cm, $P = 0.17$). The group with MVI showed significantly higher serum alpha-fetoprotein (AFP) levels (median 8.9 ng/mL, range 2.1–2022.4 ng/mL) compared with those without MVI (median 3.0 ng/mL, range 0.9–1387.3 ng/mL, $P = 0.03$).

Table 1. Clinicopathological characteristics of the patients

Characteristics	MVI (-) (n=22, %)	MVI (+) (n=14, %)	P-value**
Age (years)			
Median (range)	61.5 (35-74)	56.5 (46-73)	0.4
Sex			
Men	14 (63.6)	10 (71.4)	0.6
Women	8 (36.4)	4 (28.6)	
Staging of hepatic fibrosis*			
0	1	0	0.6
1	1	1	
2	5	3	
3	6	3	
4	9	7	
Underlying liver disease			
Hepatitis B	16 (72.7)	12 (85.7)	0.4
Hepatitis C	2 (9.1)	2 (14.3)	
Alcoholism	2 (9.1)	0 (0)	
Non B Non C	2 (9.1)	0 (0)	
Edmondson-Steiner grade of HCC			
I	7	1	0.06
II	12	7	
III	3	6	
AFP level (ng/ml)			
Median (range)	3.02 (0.9-1387.3)	8.89 (2.11-2022.37)	0.03
PIVKA-II level (mAU/ml)			
Median (range)	32 (16-827)	66 (0.74-6168)	0.09

Abbreviations: MVI, microvascular invasion; AFP, Alpha-fetoprotein; PIVKA-II, Protein induced by vitamin K absence or antagonist-II; SD, standard deviation.

* A staging system for chronic hepatitis by the Korean Study Group for the Pathology of Digestive Diseases was used (0, no fibrosis; 1, portal fibrosis; 2, periportal fibrosis, 3, septal fibrosis; 4, cirrhosis).

** Continuous data were assessed using Mann-Whitney test while categorical variables were analyzed using chi square test. Staging of hepatic fibrosis, underlying liver disease, Edmondson-Steiner grade of HCC were compared as follows; stage 4 vs. stage 0-3, hepatitis B vs. others, grade III vs. grade I-II.

Comparisons of volumetric DECT parameters between groups with and without MVI

The NICs of outer layer 1, outer layer 2, VOI_{O1}, and VOI_{O2} were significantly higher in the MVI group than in the MVI absent group ($P < 0.05$ for all, Table 2). Other layers and VOIs showed no significant differences in NIC values between the two groups ($P > 0.05$, Table 2).

For entire volumetric HCCs, quantitative parameters including total volume, maximal diameter, mean HU in mixed-energy images, lesion-to-normal parenchyma ratio of mean attenuation value, total iodine concentration, and NIC showed no difference between HCCs with and without MVI ($P > 0.05$).

Table 2. The normalized iodine concentrations of peritumoral and intratumoral regions between MVI absent and MVI present groups.

Layer thickness	Region	NIC (mg/ml)		
		MVI(-) (n=22)	MVI(+) (n=14)	P-value
2mm	Outer layer 1	0.07 ± 0.03	0.10 ± 0.03	0.01
	Outer layer 2	0.05 ± 0.03	0.07 ± 0.03	0.04
	Inner layer 1	0.12 ± 0.07	0.16 ± 0.04	0.10
	Inner layer 2	0.15 ± 0.08	0.19 ± 0.07	0.17
	VOI_{O1}	0.11 ± 0.05	0.14 ± 0.03	0.02
	VOI_{O2}	0.09 ± 0.04	0.12 ± 0.03	0.02
	VOI_{I1}	0.15 ± 0.08	0.19 ± 0.07	0.19

Abbreviations: MVI, microvascular invasion; NIC, normalized iodine concentration; VOI, volume of interest.

Values are presented in means ± standard deviations.

* Data which was obtained in part of the patient group was excluded (VOI_{I2}, n = 33).

Diagnostic performance of volumetric DECT parameters versus qualitative features for identifying MVI

The AUCs of NICs of layers and VOIs ranged from 0.67 to 0.75 (Table 3, Figure 4). The largest AUC was obtained in the NIC of outer layer 1 (0.75). A sensitivity of 78.6% and specificity of 68.2% were obtained at cutoff values of 0.082. There were no significant differences between areas in a pairwise comparison of ROC curves among layers and VOIs (all $P > 0.05$).

Table 3. The diagnostic performance of normalized iodine concentrations (NICs) of peritumoral and intratumoral regions and qualitative features for predicting MVI.

	NIC							Qualitative features	
	Outer layer 1	Outer layer 2	Inner layer 1	Inner layer 2	VOI_{O1}	VOI_{O2}	VOI_{I1}	Peritumoral enhancement	Non-smooth tumor margins
AUC	0.75	0.71	0.70	0.68	0.73	0.74	0.67	0.64	0.63
95% CI	0.58-0.91	0.53-0.89	0.52-0.87	0.50-0.85	0.57-0.90	0.58-0.91	0.49-0.85	0.45–0.83	0.44–0.82

Abbreviations: AUC, area under the ROC curve; CI, confidence interval; VOI, volume of interest.

* Data which was obtained in part of the patient group was excluded (VOI_{I2}, n = 33).

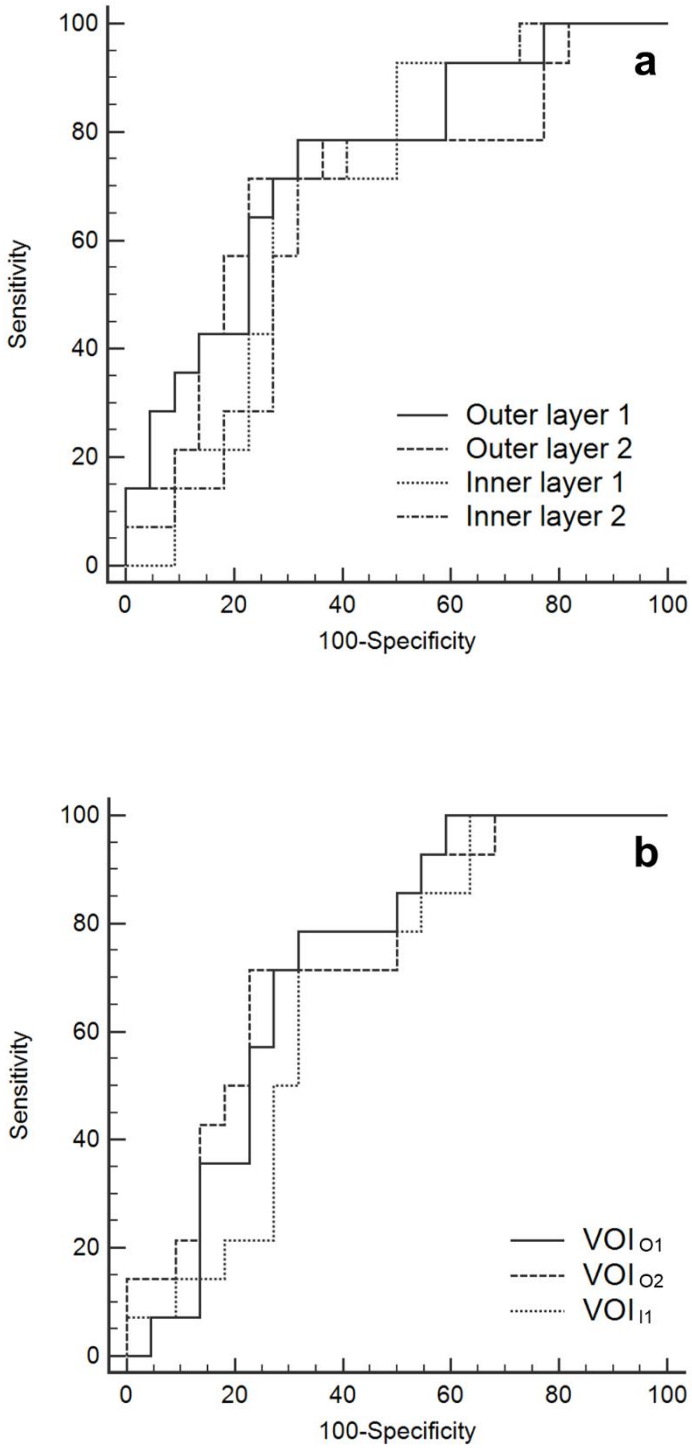

Figure 4. Receiver operating characteristic curves to evaluate the diagnostic performance of normalized iodine concentrations of peritumoral regions to identify microvascular invasion in (a) layers and (b) volume of interests.

Peritumoral enhancement of HCCs was present in 36.4% (8/22) of HCCs without MVI and in 64.3% (9/14) of HCCs with MVI. The MVI absent group showed non-smooth tumor margins in 45.5% (10/22), while the MVI present group showed 71.4% (10/14). There were no significant differences between the groups with and without MVI in peritumoral enhancement and non-smooth tumor margins (P = 0.10, 0.13). The AUCs of peritumoral enhancement and non-smooth tumor margin were 0.64 (95% CI 0.45–0.83) and 0.63 (95% CI 0.44–0.82), respectively. The AUCs of the NICs and qualitative image features showed no significant differences (P > 0.05).

Multivariate analysis of clinicopathological findings and peritumoral iodine concentration for identifying MVI

In univariate analysis, the MVI group showed more frequent abnormal protein induced by vitamin K absence or antagonist-II (PIVKA-II) level (P = 0.05), larger maximal diameter (P = 0.04), and higher NIC of outer layer 1 (P = 0.02) than the MVI absent group. In multivariate analysis, NIC of outer layer 1 was the only independent factor for predicting MVI, with an odds ratio of 7.14 (P = 0.04, Figure 5–6). The serum PIVKA-II level, Edmondson-Steiner grade, and maximal diameter were not significant predictive factors in both sets of multivariate regression analyses (P > 0.05, Table 4).

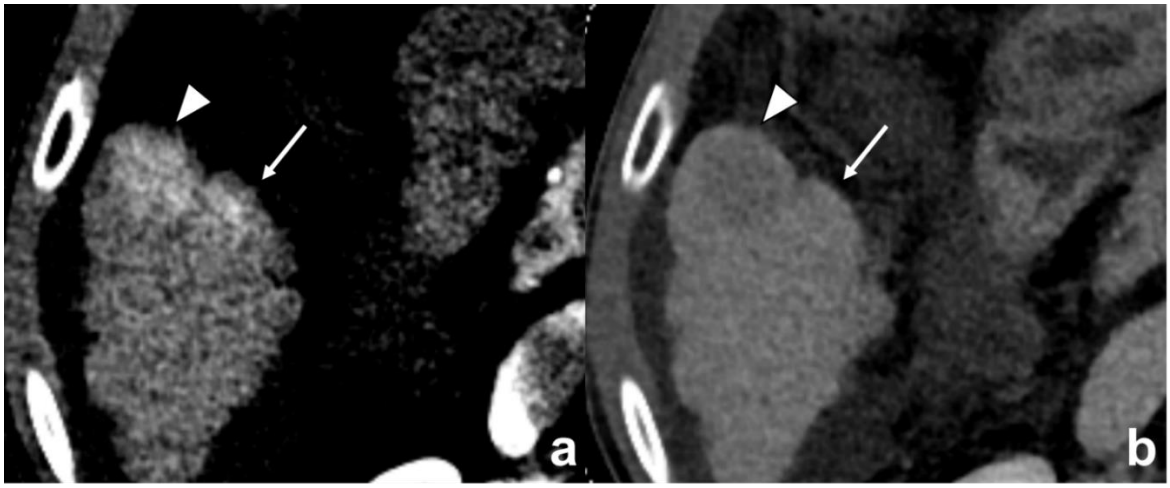

Figure 5. A 64-year-old man with hepatocellular carcinoma (HCC) without microvascular invasion (MVI). (a) Enhancing area found in the peritumoral area (arrows) adjacent to the HCC (arrowheads) in the arterial phase, which became (b) isoattenuation in the equilibrium phase. However, the NIC of the peritumoral layer with a 2-mm distance from the tumor margin is 0.03 mg/mL, lower than 0.082 mg/mL, which is the cutoff value for identifying MVI.

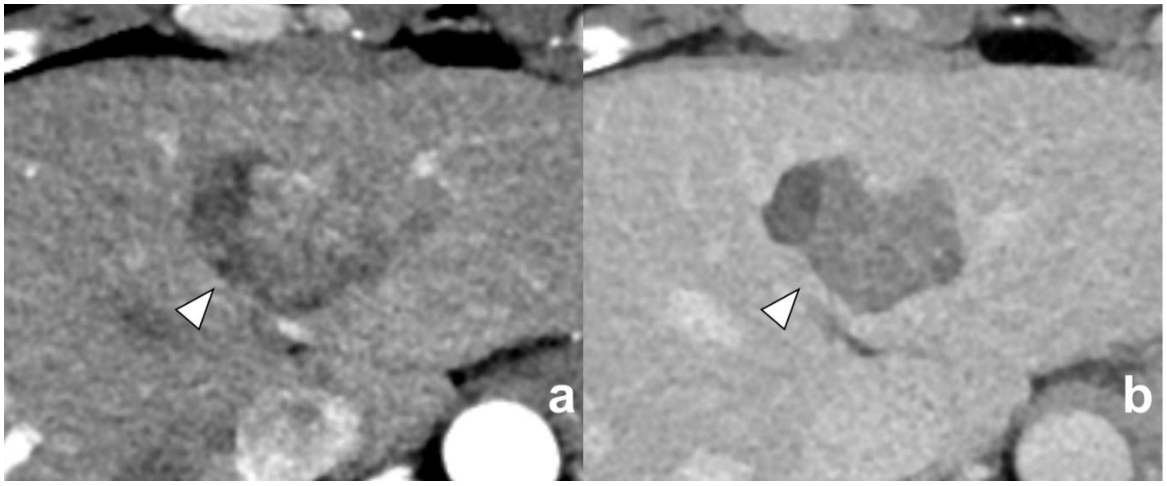

Figure 6. A 54-year-old man with hepatocellular carcinoma (HCC) with microvascular invasion (MVI). (a) No definite peritumoral enhancement found around HCC (arrowheads) in the arterial phase compared with (b) equilibrium phase images. However, the NIC of the peritumoral layer with a 2-mm distance from the tumor margin is 0.096 mg/mL, which is higher than the cutoff value for predicting MVI of 0.082 mg/mL.

Table 4. Univariate and multivariate analyses of clinical and CT parameters in predicting MVI.

Parameters	Univariate analysis		Multivariate analysis	
	Odds ratio (95% CI)	P-value	Odds ratio (95% CI)	P-value
Age (> 60years)	0.63 (0.16-2.41)	0.50		
Sex (Female)	0.70 (0.16-2.98)	0.63		
Staging of hepatic fibrosis (Stage 4)	1.44 (0.38-5.57)	0.59		
AFP (> 8.7ng/ml)	2.67 (0.65-10.88)	0.17		
PIVKA-II (> 40 mAU/mL)	4.38 (1.03-18.63)	0.05	2.71 (0.47-15.58)	0.26
Edmondson-Steiner grade of HCC (III)	4.75 (0.95-23.85)	0.06	5.64 (0.67-47.25)	0.11
Total volume of HCC (> 4.5ml)	2.16 (0.54-8.57)	0.27		
Maximal diameter of HCC (> 32mm)	4.53 (1.06-19.41)	0.04	4.04 (0.67-24.37)	0.13
Peritumoral enhancement	3.15 (0.78-12.73)	0.11		
Nonsmooth tumor margin	3.00 (0.72-12.55)	0.13		
NIC of outer layer 1 (> 0.082mg/ml)	6.42 (1.37-30.05)	0.02	7.14 (1.12-45.40)	0.04

Abbreviations: MVI, microvascular invasion; AFP, Alpha-fetoprotein; PIVKA-II, Protein induced by vitamin K absence or antagonist-II; NIC, normalized iodine concentration; VOI, volume of interest; CI, confidence interval.

Relationship between peritumoral enhancement and volumetric DECT parameters of the peritumoral layers

Layer-to-normal parenchyma ratio of mean HU values was significantly higher in outer layer 2, in both 2-mm and 4-mm layer thickness, in HCCs with peritumoral enhancement than in those in HCCs without peritumoral enhancement ($P = 0.03$, $P = 0.04$, respectively). However, the mean HU and NIC showed no significant difference between the two groups ($P > 0.05$, Table 5).

Table 5. Relationship between peritumoral enhancement and quantitative parameters of peritumoral layers.

Abbreviations: VOI, volume of interest; HU, Hounsfield unit; NIC, normalized iodine concentration.

Layer thickness	Region	Parameters	Peritumoral enhancement (-) (n = 19)	Peritumoral enhancement (+) (n = 17)	P-value
2mm	Outer layer 1	Mean HU	74.4 ± 10.6	80.4 ± 13.6	0.21
		Layer-to-normal parenchyma ratio of mean HU	1.02 ± 0.08	1.08 ± 0.12	0.09
		NIC	0.08 ± 0.04	0.09 ± 0.03	0.36
	Outer layer 2	Mean HU	76.9 ± 12.2	85.6 ± 12.9	0.07
		Layer-to-normal parenchyma ratio of mean HU	1.05 ± 0.12	1.15 ± 0.11	0.03
		NIC	0.06 ± 0.03	0.06 ± 0.03	0.57
4mm	Outer layer 1	Mean HU	74.5 ± 10.2	77.6 ± 12.0	0.68
		Layer-to-normal parenchyma ratio of mean HU	1.02 ± 0.05	1.04 ± 0.09	0.85
		NIC	0.07 ± 0.03	0.07 ± 0.03	0.53
	Outer layer 2	Mean HU	75.2 ± 10.2	82.1 ± 13.6	0.15
		Layer-to-normal parenchyma ratio of mean HU	1.03 ± 0.09	1.10 ± 0.11	0.04
		NIC	0.04 ± 0.02	0.05 ± 0.03	0.66

Diagnostic performance of peritumoral NICs versus peritumoral CT attenuations for identifying MVI

The mean attenuations of all layers and VOIs showed no significant difference between the two groups (P > 0.05, Table 6). The AUCs of the mean attenuations of layers and VOIs ranged from 0.56 to 0.66. They were not significantly different from the AUCs of NICs in pairwise comparisons (all P > 0.05).

Table 6. The Hounsfield units of peritumoral and intratumoral regions between MVI absent and MVI present groups.

Layer thickness	Region	Hounsfield unit		
		MVI(-) (n=22)	MVI(+) (n=14)	P-value
2 mm	Outer layer 1	74.4 ± 11.6	81.8 ± 12.4	0.08
	Outer layer 2	78.4 ± 13.4	85.1 ± 12.1	0.14
	Inner layer 1	97.0 ± 22.9	104.8 ± 23.0	0.33
	Inner layer 2	105.4 ± 27.7	112.4 ± 33.9	0.50
	VOI_{O1}	90.3 ± 17.5	97.1 ± 15.8	0.24
	VOI_{O2}	84.5 ± 13.1	91.7 ± 12.2	0.11
	VOI_{I1}	105.0 ± 27.8	111.4 ± 33.9	0.54
4 mm	Outer layer 1	73.4 ± 10.1	80.0 ± 11.5	0.08
	Outer layer 2	75.7 ± 11.8	82.7 ± 12.2	0.09
	Inner layer 1	100.0 ± 24.3	107.2 ± 25.3	0.40
	VOI_{O1}	84.5 ± 13.1	91.7 ± 12.2	0.11
	VOI_{O2}	78.9 ± 10.3	86.2 ± 11.0	0.05

Abbreviations: MVI, microvascular invasion; NIC, normalized iodine concentration; VOI, volume of interest.

Values are presented in means ± standard deviations.

* Data which was obtained in part of the patient group was excluded (VOI_{I2} [2mm], n = 33; Inner layer 2 [4mm], n = 33; VOI_{I1} [4mm], n = 33; VOI_{I2} [4mm], n = 14).

Effect of layer thickness

In the 4-mm layer thickness, the NICs of outer layer 1, VOI_{O1}, and VOI_{O2} were also significantly higher in the MVI group than in the MVI absent group (all $P < 0.05$, Table 7). The AUCs of the NICs ranged from 0.69 to 0.75. The largest AUC was obtained for VOI_{O2} (AUC 0.75). There

were no significant differences between areas in a pairwise comparison of ROC curves, including the values obtained in 2-mm layer thickness (all $P > 0.05$).

Table 7. The normalized iodine concentration (NICs) of peritumoral and intratumoral regions in 4mm layer thickness between MVI absent and MVI present groups.

Layer thickness	Region	NIC (mg/ml)		
		MVI(-) (n=22)	MVI(+) (n=14)	P-value
4mm	Outer layer 1	0.06 ± 0.03	0.08 ± 0.03	0.03
	Outer layer 2	0.04 ± 0.02	0.06 ± 0.03	0.05
	Inner layer 1	0.13 ± 0.07	0.17 ± 0.05	0.06
	VOI_{O1}	0.09 ± 0.04	0.12 ± 0.03	0.02
	VOI_{O2}	0.06 ± 0.03	0.09 ± 0.03	0.01

Abbreviations: MVI, microvascular invasion; NIC, normalized iodine concentration; VOI, volume of interest.

Values are presented in means ± standard deviations.

* Data which was obtained in part of the patient group was excluded (Inner layer 2, n = 33; VOI_{I1}, n = 33; VOI_{I2}, n = 14).

Intra- and interobserver agreements

Interobserver and intraobserver agreements were excellent in all measured quantitative parameters (ICC = 0.81–1.0, 0.85–1.0). In qualitative parameters, interobserver and intraobserver agreements were good to excellent and excellent, respectively (κ = 0.67–0.71, 0.78–0.89, Table 8).

Table 8. Intraobserver and interobserver agreements of quantitative and qualitative parameters.

	Qualitative features		DECT parameters of volumetric HCCs					Mean HU and NIC of layers and VOIs			
								2mm layer thickness		4mm layer thickness	
	Peritumoral enhancement	Non-smooth tumor margins	Total volume (ml)	Maximal diameter (mm)	Mean HU (HU)	Total iodine concentration (mg/ml)	NIC (mg/ml)	Layers	VOIs	Layers	VOIs
Inter-observer agreement	.67	.71	.99	.99	.99	.99	.99	.81-.99	.99-1.0	.99-1.0	.99-1.0
Intra-observer agreement	.89	.78	.99	.99	.99	.99	.99	.85-.99	.99-1.0	.99-1.0	.99-1.0

Abbreviations: DECT, dual-energy computed tomography; HCC, hepatocellular carcinoma; HU, Hounsfield unit; NIC, normalized iodine concentration; VOI, volume of interest.

* Agreements regarding categorical and continuous variables were assessed with Cohen's κ statistics and intra-class correlation coefficients (ICC), respectively

Discussion

Our study demonstrated that the NIC of the peritumoral zones and intratumoral zones of HCCs measured by DECT was useful for the prediction of MVI. In more detail, outer layer 1 and outer layer 2, which corresponded to the peritumoral layers, showed significantly higher NIC in the MVI present group than in the MVI absent group. Interestingly, the combination of HCCs and peritumoral regions (VOI_{O1}, VOI_{O2}) also showed different NIC values between the MVI present and absent groups with comparable AUCs to those of peritumoral regions only. This might imply that MVI status could be predicted by analyzing NICs of both intratumoral and peritumoral regions as well as peritumoral regions only. We also found that the NIC of the peritumoral region up to 2 mm from the tumor margin was an independent predictive factor for MVI in multivariate analysis. Yang et al. indicated that the NICs of HCCs with MVI were significantly higher than those of HCCs without MVI (18). However, our results showed no significant difference in the NICs of HCCs between the two groups. This discrepancy may have contributed to the difference in the way ROI was placed. A previous study drew the ROI with a diameter of half of the tumor size in one axial image, whereas we segmented the whole volume of the HCCs in three dimensions, which better reflects the nature of the tumor.

Peritumoral enhancement is usually defined as grossly contrast material enhancement outside of the tumor border at the arterial phase that becomes isointense with background liver parenchyma in the later dynamic phase images (19). This imaging finding probably relates to the known hypothesis of hemodynamic perfusion changes existing in compensatory arterial hyperperfusion, which can occur in the region of decreased portal flow caused by minute portal branch occlusion because of tumor thrombi, assuming that the draining veins of HCCs are usually portal venules (20). Until now, there has been controversy as to whether there is a correlation between peritumoral enhancement in CT and MVI of HCCs. Previous studies have demonstrated that peritumoral enhancement significantly

increases the risk of MVI, and the area of peritumoral hemodynamic change in HCC patients with microscopic portal invasion was significantly larger than those without it in combined CT hepatic arteriography and CT arterioportography (21, 22). However, another study by Chou et al. described peritumoral enhancement in CT was not a significant risk factor for MVI (16). One of the potential reasons for these discrepancies among the previous studies could be the qualitative assessment of peritumoral enhancement, ROI measurement of attenuation coefficient, and heterogeneous scanning parameters. Although qualitative image findings such as peritumoral enhancement and non-smooth tumor margins showed similar AUCs compared with those of NICs in our study, there were no significant factors in univariate analysis for predicting MVI, in contrast to previous studies (7, 9, 16, 17, 22). The number of patients might be insufficient to evaluate these multiple qualitative imaging features. However, the NIC of the peritumoral layer was an independent predictive factor for MVI in this setting, which suggests an additional value for MVI prediction in preoperative imaging. The diagnostic accuracy of our study (AUC 0.67–0.75, sensitivity 78.6%, specificity 68.2%) was comparable to that of a recent study that evaluated peritumoral enhancement qualitatively in CT (accuracy 74.3%) (22).

In our study, despite the attenuation coefficients of peritumoral areas showing similar AUCs compared with those of peritumoral NICs, there were no significant factors for the prediction of MVI. A previous study revealed that dual-energy CT demonstrated a linear relationship with low relative error (less than 10%) between measured and actual iodine concentrations in an in vitro experiment (23). Based on our study results, we suggest that the iodine concentration calculated using dual-energy CT may reflect peritumoral perfusional changes caused by microcirculation of the blood flow more accurately than attenuation measurements.

The main issue of our study was how to correctly draw the tumor boundary. The initial process for tumor segmentation is the most important step because it affects all of the peritumoral layers and intratumoral layers in the following process. The manual drawing in each slice is simple

but takes a lot of time and effort, and it is challenged by poor inter-reader agreement. A recent study demonstrated that semiautomatic segmentation of liver metastases in CT showed high accuracy with 82.3% of median overlap, 6.0 % overestimation ratio, and 11.5% underestimation ratio (24). We also used a dedicated software prototype (eXamine: “DE Tumor Segmentation”) that allows for a refined volumetric semiautomatic segmentation of the entire tumor and a respective evaluation of spectral data. This application is designed to evaluate different parameters of a tumor scanned with Siemens DECT technology using an iodine contrast agent. It also provides semiautomatic segmentation of the tumor peel datasets. Once the user selects the number of peels in the prototype, the user obtains the respective number of peels to the outside and inside of the original tumor automatically and a respective analysis of the different layers from a spectral perspective. Although we had to edit the tumor margins manually in a few HCCs with ill-defined margins, most tumors were segmented accurately and efficiently. This process minimized the hand-related artifacts and showed excellent intra- and interobserver agreements. The layer thickness (2 mm or 4 mm) did not affect the diagnostic performance in our study. This result suggests that perfusional change occurs in the peritumoral region within a distance of at least 8 mm from the tumor margin.

This study has some limitations. First, this retrospective study was performed in a single center with a small number of patients. Additionally, only surgically confirmed HCCs were included in this study. A potential selection bias might have occurred. However, because MVI can only be confirmed by pathology, strict inclusion criteria are inevitable. Second, tumors less than 1 cm were excluded from our study because of the potential measurement error. Although it was not intended, all HCCs of the patients were less than 5 cm in maximal diameter. Therefore, our results cannot be generalized to small (<1 cm) or large (>5 cm) HCCs. Third, the software used in our study was only available in dual-source dual-energy CT. Other dual-energy techniques, such as rapid kVp switching or dual-layer spectral CT, were not used in our study. Further studies using other dual-energy CT vendors are warranted.

In conclusion, the volumetric iodine quantification of peritumoral regions will be useful for predicting MVI in preoperative dual-energy CT.

Reference

1. Omata M, Cheng AL, Kokudo N, et al. Asia-Pacific clinical practice guidelines on the management of hepatocellular carcinoma: a 2017 update. Hepatol Int. 2017;11(4):317-370.
2. Bruix J, Gores GJ, Mazzaferro V**.** Hepatocellular carcinoma: clinical frontiers and perspectives. Gut. 2014;63(5):844-855.
3. Llovet JM, Schwartz M, Mazzaferro V**.** Resection and liver transplantation for hepatocellular carcinoma. Semin Liver Dis. 2005;25(2):181-200.
4. Zimmerman MA, Ghobrial RM, Tong MJ, et al. Recurrence of hepatocellular carcinoma following liver transplantation: a review of preoperative and postoperative prognostic indicators. Arch Surg. 2008;143(2):182-188.
5. Imamura H, Matsuyama Y, Tanaka E, et al. Risk factors contributing to early and late phase intrahepatic recurrence of hepatocellular carcinoma after hepatectomy. J Hepatol. 2003;38(2):200-207.
6. Ahn SY, Lee JM, Joo I, et al. Prediction of microvascular invasion of hepatocellular carcinoma using gadoxetic acid-enhanced MR and (18)F-FDG PET/CT. Abdom Imaging. 2015;40(4):843-51.
7. Renzulli M, Brocchi S, Cucchetti A, et al. Can current preoperative imaging be used to detect microvascular invasion of hepatocellular carcinoma? Radiology. 2016;279(2):432-442.
8. Ariizumi S-i, Kitagawa K, Kotera Y, et al. A non-smooth tumor margin in the hepatobiliary phase of gadoxetic acid disodium (Gd-EOB-DTPA)-enhanced magnetic resonance imaging predicts microscopic portal vein invasion, intrahepatic metastasis, and early recurrence after hepatectomy in patients with hepatocellular carcinoma. J Hepatobiliary Pancreat Sci. 2011;18(4):575-585.
9. Segal E, Sirlin CB, Ooi C, et al. Decoding global gene expression programs in liver cancer by noninvasive imaging. Nat Biotechnol. 2007;25(6):675-680.

10. Lee S, Kim SH, Lee JE, et al. Preoperative gadoxetic acid-enhanced MRI for predicting microvascular invasion in patients with single hepatocellular carcinoma. J Hepatol. 2017;67(3):526-534.
11. Goo HW, Goo JM**.** Dual-energy CT: new horizon in medical imaging. Korean J Radiol. 2017;18(4):555-569.
12. Agrawal MD, Pinho DF, Kulkarni NM, et al. Oncologic applications of dual-energy CT in the abdomen. Radiographics. 2014;34(3):589-612.
13. De Cecco CN, Darnell A, Rengo M, et al. Dual-energy CT: oncologic applications. AJR Am J Roentgenol. 2012;199(Suppl 5):S98-S105.
14. Baxa J, Matouskova T, Krakorova G, et al. Dual-phase dual-energy CT in patients treated with erlotinib for advanced non-small cell lung cancer: possible benefits of iodine quantification in response assessment. Eur Radiol. 2016;26(8):2828-2836.
15. Park YN, Kim Hg, Chon CY, et al. Histological grading and staging of chronic hepatitis standardized guideline proposed by the Korean study group for the pathology of digestive diseases. J Pathol Transl Med. 1999;33(5):337-346.
16. Chou CT, Chen RC, Lin WC, et al. Prediction of microvascular invasion of hepatocellular carcinoma: preoperative CT and histopathologic correlation. AJR Am J Roentgenol. 2014;203(3):W253-W259.
17. Chou CT, Chen RC, Lee CW, et al. Prediction of microvascular invasion of hepatocellular carcinoma by pre-operative CT imaging. Brit J Radiol. 2012;85(1014):778-783.
18. Yang CB, Zhang S, Jia YJ, et al. Dual energy spectral CT imaging for the evaluation of small hepatocellular carcinoma microvascular invasion. Eur J Radiol. 2017;95:222-227.
19. An C, Kim DW, Park YN, et al. Single hepatocellular carcinoma: preoperative MR imaging to predict early recurrence after curative resection. Radiology. 2015;276(2):433-443.
20. Matsui O, Kobayashi S, Sanada J, et al. Hepatocelluar nodules in liver cirrhosis: hemodynamic evaluation (angiography-assisted CT) with special reference to multi-step

hepatocarcinogenesis. Abdom Imaging. 2011;36(3):264-272.

21. Nishie A, Yoshimitsu K, Asayama Y, et al. Radiologic detectability of minute portal venous invasion in hepatocellular carcinoma. AJR Am J Roentgenol. 2008;190(1):81-87.

22. Xu X, Zhang HL, Liu QP, et al. Radiomic analysis of contrast-enhanced CT predicts microvascular invasion and outcome in hepatocellular carcinoma. J Hepatol. 2019;70(6):1133-1144.

23. Lv P, Lin XZ, Li J, et al. Differentiation of small hepatic hemangioma from small hepatocellular carcinoma: recently introduced spectral CT method. Radiology. 2011;259(3):720-729.

24. Yan J, Schwartz LH, Zhao B**.** Semiautomatic segmentation of liver metastases on volumetric CT images. Med Phys. 2015;42(11):6283-6293.

요약 (국문초록)

간세포암의 미세혈관침습 예측: 수술 전 이중에너지 전산화 단층촬영을 이용한 용적화된 요오드 정량화의 가치

서울대학교 의과대학원

임상의과학과

김택민

연구 목적

본 연구는 수술 전 이중에너지 CT 를 이용한 용적화된 요오드 정량화를 통해 간세포암의 미세혈관 침습을 예측하는 것을 목적으로 하였다.

연구 방법

수술 전 이중에너지 CT 를 촬영하고 수술적 제거로 간세포암으로 확진된 환자들이 후향적으로 본 연구에 포함되었다. 동맥기에서 대동맥을 기준으로 표준화 된 요오드 농도 (normalized iodine concentration, NIC)와 혼합 에너지에서의 CT 감쇠계수를 포함한 이중에너지 CT 의 정량적인 특성들을 종양 주변 지역과 종양 내부

지역에서 삼차원적으로 측정하였다. 이를 통해 (i) 2 mm 층 두께로 나눈 종양 주변의 층들 (outer layers 1 과 2; 종양 경계에서 가까운 순서대로 번호 매김)과 종양 내부의 층들 (inner layers 1 과 2) 간의 층-대-층 (layer-by-layer) 분석과 (ii) 5 개의 용적 적용 범위 (종양 자체; VOI_{O1}, 종양과 outer layer 1 을 더한 부피; VOI_{O2}, 종양과 outer layers 1 과 2 을 더한 부피; VOI_{I1}, 종양에서 inner layer 1 을 뺀 부피; VOI_{I2}, 종양에서 inner layers 1 과 2 를 뺀 부피) 를 사용한 volume of interest (VOI) 기반 분석을 시행하였다. 추가적으로 종양 주변 지역의 조영증강과 종양의 경계 모양을 포함한 정성적 분석을 시행하였다. 미세혈관 침습이 있는 간세포암과 미세혈관 침습이 없는 간세포암, 두 군에서 정량적, 정성적인 CT 특성들을 비교하였다. 층과 VOI 들의 이중에너지 CT 특성들은 수신자 조작 특성 (receiver operating characteristic, ROC) 곡선 분석을 통해 진단적 가치를 평가하였다. 일변량 분석에서 유의한 결과를 얻은 변수들은 다변량 분석을 시행하였다.

연구 결과

미세혈관 침습이 있는 14 명의 환자와 미세혈관 침습이 없는 22 명의 환자를 포함한 총 36 명의 환자 (남자 24 명, 평균 나이 59.9 ± 8.5 세) 가 최종적으로 포함되었다. Outer layer 1, outer layer 2, VOI_{O1}, VOI_{O2} 의 NIC 가 미세혈관 침습이 있는 환자군에서 유의하게 높게 측정되었다 ($P < 0.05$). 층과 VOI 들의 NIC 중에서 outer layer 1 의 NIC 가 곡선 아래 영역 (area under the curve, AUC) 이 0.747 로 가장 높았다. 종양 주변 지역의 조영증강, 종양의 경계와 같은 정성적인 특성들과 층과 VOI 의 CT 감쇠 계수는 미세혈관 침습이 있는 군와 없는 군 간에 유의한 차이를 보이지 않았다 ($P > 0.05$). 다변량 분석에서 outer layer 1 의 NIC 는 미세혈관 침습을 예측하는 데 있어 독립적인 인자로 밝혀졌다 (위험도 7.14, $P = 0.04$).

결론

수술 전 이중에너지 CT 를 사용한 종양 주변 지역과 종양 내부 지역의 용적화된 요오드 정량화는 간세포암의 미세혈관 침습 여부과 연관이 있었으며, 이를 예측하는 데 유용하게 쓰일 것으로 보인다.

주요어

간세포암, 미세혈관 침습, 이중에너지 전산화 단층촬영, 종양 주변 지역 조영증강, 요오드 정량화, 요오드 농도.

학번: 2017-20656